Simple, portable, and low-cost microscope based on off-axis digital holography using two spherical waves

Yujie Lu, Yunhui Liu,* and Tak Kit Lau

Department of Automation and Mechanical Engineering, The Chinese University of Hong Kong, Shatin, N.T. 999077, Hong Kong, China

**Corresponding author: yhliu@mae.cuhk.edu.hk*

Received June 13, 2014; accepted June 26, 2014;
posted July 2, 2014 (Doc. ID 213818); published July 29, 2014

In this Letter, we present a highly compact and low-cost holographic microscope which is especially suitable for observing transparent samples with certain specific supports such as microchannels. This microscope employs only an inexpensive laser diode, a dual precision round aperture, and a digital light sensor. The total cost of the system except for the digital sensor is less than 400 US dollars, and a hand-held system can be made based on our setup. Besides the simple, cheap, and compact setup, this system can capture the off-axis interference pattern of two spherical waves and reconstruct the quantitative phase profile along with the amplitude image of the observed sample with the twin image eliminated in real time. Experimental results show that the resolution of our system is better than 2 μm, and the 3D structure of blood cells can be retrieved.

OCIS codes: (090.1995) Digital holography; (120.5050) Phase measurement; (090.2880) Holographic interferometry.
http://dx.doi.org/10.1364/OL.39.004549

Gabor in-line holography was first introduced in 1948 [1]. Microscopes based on Gabor in-line holography can be made cheaply and compactly [2–4]. However, this method suffers significantly from the twin image which smears around the object, lowering the contrast of the reconstructions. Even though iteration algorithms [2,5] can effectively suppress the twin image, it is time-consuming for real-time imaging systems, and the size of the sample is restricted by the Fresnel number of the recording geometry. Off-axis holography [6–8], on the other hand, generates high-quality images and retrieves quantitative phase images but is much more complicated. Researchers employ beam splitters, mirrors, condensers, and lenses to gain enlarged off-axis holograms, which greatly increase the cost and size of the whole system. Recently, great efforts were made to lower the cost of the off-axis holographic microscope [9–11], where diverse brilliant holographic interferometers were invented. However, all of those interferometers were required to be installed on a traditional optical microscope, leading to an expanded size of those systems. This Letter aimed to design a low-cost and more compact off-axis holographic transmission microscope which has a simple setup as in Gabor in-line holography but features characteristics of off-axis holography.

The schematic of the system is shown in Fig. 1. Except for the dual aperture (customized from National Aperture, pinhole size = 5 μm, center to center distance = 1.7 mm), the geometry of our system is similar to Gabor in-line holography where the object is a few millimeters away from the point source, and the digital light sensor is several times farther away. An inexpensive laser diode (LD-T650H00, $\lambda = 650$ nm, measured power ≈120 mW) casts a light spot on the dual aperture which produces two coherent spherical light sources. The first point source, emitted from the object pinhole, illuminates on the object, while the other one, emitted from the reference pinhole, illuminates a clean area to create the reference wave. The two beams interfere with each other at the sensor plane to create a hologram which is then captured by the digital sensor (ORIA-2-CL-M-S, resolution: $2048 * 2048$, pixel size = 5.5 μm). This gray-scale hologram can be represented as

$$I = |R_1(x,y) + O_1(x,y)|^2. \tag{1}$$

$R_1(x,y)$ is the wavefront of the reference wave at the digital sensor plane, and $O_1(x,y)$ is that of the object wave. The reference wave in this Letter refers in particular to the off-axis reference wave, and the object wave is the combination of the in-line reference wave and the in-line object wave. The reference wave can be treated as an ideal point source such that

$$R_1(x,y) = |R_1(x,y)| \exp(ikr_{R1}), \tag{2}$$

where k is the wave number and $r_{R1} = \sqrt{(x-x_{p0})^2 + (y-y_{p0})^2 + Z^2}$. The object wave, however, is modulated by the object. According to the Huygens–Fresnel principle [2,12], the wavefront of the object wave at the sensor plane can be calculated using the wavefront at the sensor plane. For simplicity, we directly give the convolution form of this principle:

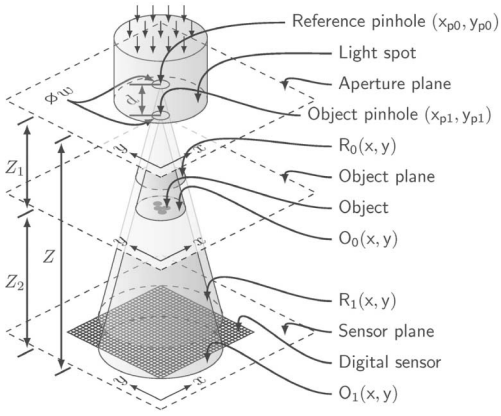

Fig. 1. System diagram.

0146-9592/14/154549-04$15.00/0

$$O_1(x,y) = O_0(x,y) ** h_{Z2}(x,y), \tag{3}$$

where $**$ is the convolution operator, $O_0(x,y)$ is the light field right after the object plane, and h_{Z2} is the Fresnel kernel, which can be defined as [12,13]

$$h_{Z2}(x,y) = \exp\left(i\frac{\pi}{\lambda Z_2}(x^2+y^2)\right). \tag{4}$$

If we treat the sample as a planar object, the light field right after the object plane can be regarded as the combination of original in-line reference wave and the in-line object wave such that

$$O_0(x,y) = (1+f(x,y))\exp(ikr_{O0}). \tag{5}$$

$f(x,y)$ is the complex value of the planar sample, and $r_{O0} = \sqrt{(x-x_{p1})^2+(y-y_{p1})^2+Z_1^2}$. If we use a quadratic-phase exponential to approximate the wavefronts of the object wave [12,14] and substitute Eq. (5) into Eq. (3), we can simplify the expression of $O_1(x,y)$ using operators (Q, R, and V) defined in Section 5.4.1 of [12] as follows:

$$\begin{aligned} O_1(x,y) &= ((1+f(x,y))\exp(ikr_{O0})) ** h_{Z2} \\ &\approx R[Z_2]Q\left[\frac{1}{Z_1}\right]\{(1+f(x,y))\} \\ &= Q[Z]V\left[\frac{1}{M}\right]R\left[\frac{Z_2}{M}\right]\{(1+f(x,y))\} \\ &= Q[Z]R[MZ_2]V\left[\frac{1}{M}\right]\{(1+f(x,y))\} \\ &\approx \left(\left(1+f\left(\frac{x}{M},\frac{y}{M}\right)\right) ** h_{M*Z2}(x,y)\right)\exp(ikr_{O1}), \end{aligned} \tag{6}$$

where $r_{O1} = \sqrt{(x-x_{p1})^2+(y-y_{p1})^2+Z^2}$, and the magnification factor of the system $M = Z/Z_1$. If we define

$$\begin{aligned} O_1(x,y) &= O_1(x,y)\exp(-ikr_{O1}) \\ &\approx \left(1+f\left(\frac{x}{M},\frac{y}{M}\right)\right) ** h_{M*Z2}(x,y), \end{aligned} \tag{7}$$

and substitute Eqs. (2) and (6) into Eq. (1), we can get

$$\begin{aligned} I &= |R_1(x,y)|^2 + |O_1(x,y)|^2 \\ &\quad + |R_1(x,y)|O_1(x,y)\exp[ik(r_{O1}-r_{R1})] \\ &\quad + |R_1(x,y)|O_1^*(x,y)\{\exp[ik(r_{O1}-r_{R1})]\}^*. \end{aligned} \tag{8}$$

The first two terms are the zero-order terms, while the third and forth terms are known as the object term and the twin image term, respectively. By first-order approximation, the term $\exp[ik(r_{O1}-r_{R1})]$ can be simplified as $C * \exp[(ik/Z)(d_x x + d_y y)]$, where C is a complex constant, $d_x = x_{p1} - x_{p0}$, and $d_y = y_{p1} - y_{p0}$. From this equation, we can see that the term $\exp[ik(r_{O1}-r_{R1})]$ pushes the object term and the twin image term into the higher frequency part, and the shifted frequency

$$f_{sh} \approx \frac{d}{Z\lambda}, \tag{9}$$

where d is the distance between two pinholes. Thus, we can adopt the spatial filtering method [15] used in off-axis holography with plane waves to reconstruct this hologram grabbed by our system.

The distance between two pinholes, namely d, is the only parameter which does not exist in Gabor in-line holography. Several issues need to be taken into consideration when determining the value of the d. First, d is proportional to the shifted frequency as shown in Eq. (9). If the sampling frequency of the digital sensor is fixed, the optimal frequency of the shifted frequency is fixed as demonstrated in [13,16]. Thus, d should be in line with the values of Z and λ. If d is badly decided, Z or λ should be adjusted accordingly in order to generate off-axis holograms with proper fringes, which may influence the resolution of our system. Second, d restricts the minimum size of the light spot which covers the reference pinhole and the object pinhole, while the size of the light spot exerts a crucial impact on the light flux through the dual aperture. As a result, d should be small enough to ensure that sufficient light can go through the dual aperture. In the end, d influences the flexibility of our system. If d is smaller than $W/(M-1)$, where W is the side length of the digital sensor, the wavefront of the reference wave at the object plane will overlap with the object wave, which may introduce noise into the reconstructions. Among the aforementioned three issues, we think that the first one is the most important. This is because once d is determined, the maximum resolution of the proposed system is fixed no matter how we modify the other parameters. For the second and third issues, we can remedy the limitations of d by utilizing powerful lasers and microchannels.

As aforementioned, the most striking advantages of the proposed system are the capacity of the formation of off-axis holograms and the elimination of the twin image with a simple setup similar to Gabor in-line holography. To verify this characteristic, we first compared the results of the proposed system with the results of Gabor in-line holography shown in Fig. 2. Unlike the in-line hologram shown in Figs. 2(b) and 2(d), high-frequency fringes show up in Figs. 2(a) and 2(c), which represent the formation of the off-axis hologram. From the reconstructed amplitude image in Figs. 2(e) and 2(f), it can be seen that the contrast of the reconstructions using the proposed system is much higher than using Gabor in-line holography with similar configurations. Also, larger viewing area can be obtained using the proposed system. This may be because the object at the edge of the image is submerged by the smeared twin image of the central object with the in-line setup. Last but not least, lower noise can be obtained in the clean area. In contrast with enlarged amplitude image of area D shown in Fig. 2(h), smaller intensity turbulence is observed in Fig. 2(g), to which speckle noise contributes most.

The theoretical resolution of proposed system is the same as in Gabor in-line holography, which is confirmed

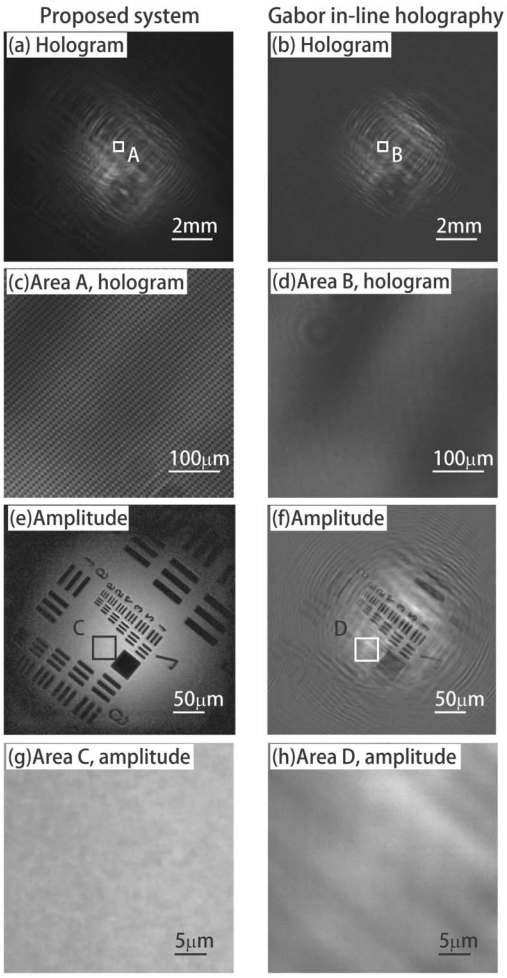

Fig. 2. Comparison of results of proposed system with results of Gabor in-line holography. Target: USAF 1951. For the proposed system, the source–sensor distance = 29 mm and the source–object distance = 1 mm (the distances shown in this Letter are calculated using the shifted frequency of the image and the distance between two pinholes); NA = 0.20. For the Gabor in-line system, the configuration is roughly the same as the proposed system.

by Fig. 3. The smallest element of USAF 1951 group 7 is clearly resolved, which implies that the resolution of our system is better than 2.19 μm. And with 3 μm apertures, we predict that the resolution of 1 μm can be easily achieved with corresponding values of Z and d. However, further improvement by increasing the NA of the system and shrinking the size of the pinholes can be found exceptionally difficult, as nearly no light can go through

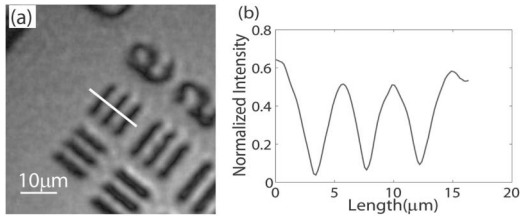

Fig. 3. Enlarged image of Fig. 2(e). The width of smallest element of USAF 1951 group 7 is 2.19 μm. A cross section of the amplitude image across the smallest bar demonstrates the resolution of proposed system to be <2.19 μm.

the dual aperture. Still, the resolution of our system can be improved using immersion holography [17].

The alignment of our system is relatively simple in comparison with Gabor in-line holography, because we do not use any microscope objective to increase the illumination angle. We just cast a large light spot on the dual aperture, which can easily cover the two pinholes. However, as almost all light is blocked by the dual aperture, we have to use a laser diode with considerably large power. Based on our experimental results, a laser diode of about 120 mW can provide enough light in our system with 3 μm pinholes.

To further demonstrate the feasibility of our system, we conducted several experiments with biological samples. Figure 4 shows 2D reconstructions of stained human stem cells. Unlike USAF 1951, which is a pure amplitude object, stem cells are not opaque. The quantitative phase profile of those stem cells along with the amplitude image can be acquired using the proposed holographic microscope. Figure 5 shows other results with blood cells. The unwrapped phase represents the optical delay of the transmissive light. When the refractive index is homogeneous inside the sample, the phase profile can reflect the 3D structure of the sample. Figure 5(d) shows the 3D rendering of the phase profile of the blood cells. As we can see, the 3D structure can be clearly obtained.

One major assumption of our system is that the reference wave illuminates a clean area. If this assumption does not hold, the twin image of the dirt which contaminates the reference wave may be seen in the reconstructions. Figure 6 shows the reconstruction results under such circumstances. In this case, the reference wave illuminates a sample which is highlighted by the black rectangle in Fig. 6(b). Thus the twin image of this sample appears at the same position in the reconstructed image at $z = 1270$ μm as shown in Fig. 6(a), and this sample can be reconstructed at the same depth in the opposite direction. This situation can be easily avoided when microchannels are used to restrict the samples. Also, fluidic samples can be pumped through the microchannel, which can greatly increase the flexibility of the system. With one core of GTX 690, the capture and 3D reconstruction of a hologram of $2048 * 2048$ takes only about 20 ms. This enables us to observe samples with

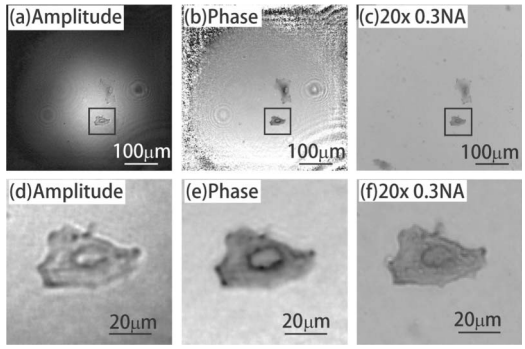

Fig. 4. Reconstruction results of human stem cells using the proposed system. A photograph captured with 20×0.3 NA lens using a traditional optical microscope is provided for comparison. Source–sensor distance = 29.4 mm; source-object distance = 1.3 mm; NA = 0.2.

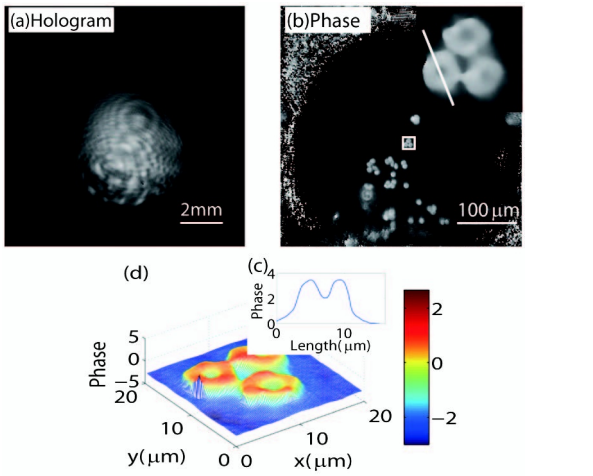

Fig. 5. Hologram of blood cells and its reconstructions. Source–sensor distance = 29.5 mm, source-object distance = 1 mm, NA = 0.2. (a) Gray-scale hologram. (b) Phase reconstructions of (a); an enlarged picture of the highlighted area is provided on the upper-right corner. (c) Phase value of the white line on (b). (d) 3D rendering of highlighted area of (b).

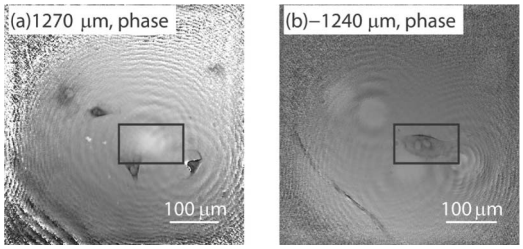

Fig. 6. Reconstructed phase image of a hologram of human stem cells (a) at 1270 μm and (b) at −1240 μm.

high throughput in real time using multiple graphics processing units (GPUs).

In conclusion, we have shown a highly compact, low-cost microscope using two spherical waves created by a dual precision aperture. The amplitude and phase profile of the sample can be retrieved using this holographic microscope. The resolution of this microscope is better than 2 μm, and 3D image of blood cells can be reconstructed in real time.

This work is supported in part by the Hong Kong Innovation and Technology Fund via project ITS/089/13 and the State Key Laboratory of Robotics and Systems, Harbin Institute of Technology.

References

1. D. Gabor, Nature **161**, 777 (1948).
2. O. Mudanyali, D. Tseng, C. Oh, S. O. Isikman, I. Sencan, W. Bishara, C. Oztoprak, S. Seo, B. Khademhosseini, and A. Ozcan, Lab Chip **10**, 1417 (2010).
3. D. Tseng, O. Mudanyali, C. Oztoprak, S. O. Isikman, I. Sencan, O. Yaglidere, and A. Ozcan, Lab Chip **10**, 1787 (2010).
4. T. Shimobaba, Y. Taniguchi, A. Shiraki, N. Masuda, and T. Ito, in *Biomedical Optics* (Optical Society of America, 2012), paper JM3A.50.
5. G. Koren, F. Polack, and D. Joyeux, J. Opt. Soc. Am. A **10**, 423 (1993).
6. E. Cuche, P. Marquet, and C. Depeursinge, Appl. Opt. **38**, 6994 (1999).
7. D. Carl, B. Kemper, G. Wernicke, and G. von Bally, Appl. Opt. **43**, 6536 (2004).
8. B. Kemper and G. von Bally, Appl. Opt. **47**, A52 (2008).
9. P. Girshovitz and N. T. Shaked, Opt. Express **21**, 5701 (2013).
10. Z. Monemhaghdoust, F. Montfort, Y. Emery, C. Depeursinge, and C. Moser, Biomed. Opt. Express **5**, 1721 (2014).
11. B. Kemper, A. Vollmer, C. E. Rommel, J. Schnekenburger, and G. von Bally, J. Biomed. Opt. **16**, 026014 (2011).
12. J. W. Goodman and S. C. Gustafson, Opt. Eng. **35**, 1513 (1996).
13. N. Verrier and M. Atlan, Appl. Opt. **50**, H136 (2011).
14. K. M. Molony, B. M. Hennelly, D. P. Kelly, and T. J. Naughton, Opt. Commun. **283**, 903 (2010).
15. E. Cuche, P. Marquet, and C. Depeursinge, Appl. Opt. **39**, 4070 (2000).
16. N. Pavillon, C. S. Seelamantula, M. Unser, and C. Depeursinge, Proc. SPIE **7723**, 77231U (2010).
17. J. Garcia-Sucerquia, W. Xu, M. Jericho, and H. J. Kreuzer, Opt. Lett. **31**, 1211 (2006).